BBA - Bioenergetics 1860 (2019) 148063

Contents lists available at ScienceDirect

BBA - Bioenergetics

journal homepage: www.elsevier.com/locate/bbabio

Structural diffusion properties of two atypical Dps from the cyanobacterium *Nostoc punctiforme* disclose interactions with ferredoxins and DNA

Vamsi K. Moparthi[a,*,1], Satish B. Moparthi[b,2], Christoph Howe[a], Patrícia Raleiras[a,3], Jerome Wenger[b], Karin Stensjö[a,*]

[a] Department of Chemistry–Ångström Laboratory, Uppsala University, SE – 751 20 Uppsala, Sweden
[b] Aix Marseille Univ, CNRS, Centrale Marseille, Institut Fresnel, Marseille, France

ARTICLE INFO

Keywords:
Cyanobacteria
Ferredoxin
Ferritin-like proteins
Fluorescence correlation spectroscopy, FCS
Iron
Protein-protein interaction

ABSTRACT

Ferritin-like proteins, Dps (DNA-binding protein from starved cells), store iron and play a key role in the iron homeostasis in bacteria, yet their iron releasing machinery remains largely unexplored. The electron donor proteins that may interact with Dps and promote the mobilization of the stored iron have hitherto not been identified. Here, we investigate the binding capacity of the two atypical Dps proteins NpDps4 and NpDps5 from *Nostoc punctiforme* to isolated ferredoxins. We report NpDps-ferredoxin interactions by fluorescence correlation spectroscopy (FCS) and fluorescence resonance energy transfer (FRET) methods. Dynamic light scattering, size exclusion chromatography and native gel electrophoresis results show that NpDps4 forms a dodecamer at both pH 6.0 and pH 8.0, while NpDps5 forms a dodecamer only at pH 6.0. In addition, FCS data clearly reveal that the non-canonical NpDps5 interacts with DNA at pH 6.0. Our spectroscopic analysis shows that [Fe−S] centers of the three recombinantly expressed and isolated ferredoxins are properly incorporated and are consistent with their respective native states. The results support our hypothesis that ferredoxins could be involved in cellular iron homeostasis by interacting with Dps and assisting the release of stored iron.

1. Introduction

Iron metabolism is one of the very early important acquisitions in the origin of life, as iron is required for cells to survive and to be functionally active [1–4]. Iron is usually found in two interconvertible oxidation states, Fe^{2+} and Fe^{3+}. However, Fe^{2+} can oxidize to Fe^{3+} in the presence of O_2. Fe^{3+} then forms iron hydroxide and precipitates, thus limiting its availability to cells. The oxidation of Fe^{2+} by H_2O_2 produces reactive oxygen species (ROS) [1], which damage crucial cell components like DNA, enzymes, and lipids. Therefore, intracellular iron homeostasis needs to be tightly regulated. Prokaryotes and eukaryotes use a family of proteins called ferritin-like proteins to regulate free Fe^{2+} concentration in the cytosol [5], found in all three domains of life. In bacteria, there are three types of ferritin-like proteins: ferritins (Ftn), bacterioferritins (Bfr), and DNA-binding proteins from starved cells (Dps) [4,6]. Ferritin-like proteins oxidize Fe^{2+} to Fe^{3+} at their ferroxidase centers (FOC), and in most, the Fe^{3+} mineral is stored in the protein core [6]. Ftn and Bfr are large protein multi-structures (24-mer) that store up to 4500 Fe ions, while Dps are dodecameric (12-mer) proteins that can store about 500 Fe ions. The common working hypothesis is that under low iron conditions, the ferric mineral core is reduced to soluble Fe^{2+}, which is released to be utilized by the cell [7–11]. This reduction step is crucial for the stored iron to re-enter the metabolism, but unfortunately, little is known about this process, and the identity of the donor that assists electron transfer into Dps is unrevealed.

Numerous studies in various bacteria have shown that Dps homologs exhibit efficient DNA protection, against damage by reactive oxygen species, partly by direct physical binding of DNA [12–18]. Therefore, DNA binding activity is considered as one of the

Abbreviations: Dps, DNA-binding proteins from starved cells; DLS, dynamic light scattering; FOC, ferroxidase centers; FRET, fluorescence resonance energy transfer; FCS, fluorescence correlation spectroscopy; EPR, electron paramagnetic resonance; Fdx, ferredoxin; EMSA, electrophoretic mobility shift assay; NpFdx, Ferredoxin from *Nostoc punctiforme*

* Corresponding authors.
E-mail addresses: vamsi.moparthi@ifm.liu.se (V.K. Moparthi), karin.stensjo@kemi.uu.se (K. Stensjö).
[1] Present address: Department of Physics, Chemistry and Biology, Division of Chemistry, Linköping University, SE-58183 Linköping, Sweden.
[2] Present address: Membrane Biochemistry and Transport, Institute Pasteur, 28 rue du Dr. Roux, 75,015, Paris, France.
[3] Present address: Medicago AB, Danmark Berga 13, SE-75598 Uppsala, Sweden.

https://doi.org/10.1016/j.bbabio.2019.148063
Received 2 March 2019; Received in revised form 6 August 2019; Accepted 10 August 2019
Available online 13 August 2019

characteristic features of Dps proteins. In contrast, mechanical DNA protection is not one of the core functions of Bfr.

Dps proteins are present in most of the cyanobacteria phyla, where they play a major role in tolerance to oxidative stress, peroxide detoxification, prevention of DNA damage and maintaining the iron homeostasis [19–22]. Unlike most other prokaryotes, which encode a single Dps, there are five genes annotated as ferritin-like proteins in the multicellular, heterocyst-forming cyanobacterium *Nostoc punctiforme* sp. *ATCC* 29133 (from here on *N. punctiforme*) [23]. We have previously asserted that these proteins co-exist, and named them NpDps1, NpDps2, NpDps3, NpDps4 and NpDps5 [21]. In a phylogenetic analysis it was shown that NpDps1-3 grouped into distinct clades of typical Dps proteins, while both NpDps4 and NpDps5 clustered with non-canonical groups of ferritin-like proteins. One atypical feature of NpDps4 was the unusual ligand sphere of the FOC, also identified in *e.g.* DpsA-Te from *Thermosynechococcus elongatus* [20,24].

Recently we resolved the structure of NpDps4, and revealed that O_2 rather than $H_2O_2$was used to oxidize the bound ferrous iron to ferric iron [25]. NpDps5 clustered with, and shared structural features with Bfr, such as harboring the FOCs within the monomers [20]. NpDps5 has been identified as involved in light tolerance in *N. punctiforme*, and an increase in NpDps5 abundance was shown to enhance tolerance to hydrogen peroxide [22], likely due to is role in iron regulation [21]. The functional roles of NpDps4 have not yet been explored. NpDps5 and NpDps4 are associated with a specific type of cell, the heterocyst, as demonstrated by transcriptional and proteomics studies [20,26]. Heterocysts are formed during nitrogen-depleted conditions in some filamentous cyanobacteria and exhibit an intracellular micro-oxic condition that enable nitrogen fixation [27]. The core enzymes involved in heterocyst metabolism are iron-dependent and O_2 sensitive. Our hypothesis is that NpDps4 and NpDps5 are involved in the strict control of iron and O_2 levels in heterocysts.

As mentioned earlier, the chemistry behind the release of ferrous iron from the mineralized iron core of Dps is largely unknown. This study aimed to identify electron transfer proteins that interact with the atypical NpDps4, and the bacterioferritin-like, NpDps5. Ferredoxins (Fdxs) are soluble electron transfer proteins found ubiquitously in organisms. They possess a highly negative redox potential and use their [Fe−S] (iron-sulfur) clusters to act as electron distributors in various metabolic pathways. Fdxs can be classified according to their [Fe−S] clusters, like [2Fe−2S], [3Fe−4S] and [4Fe−4S], and to the organisms in which they were first isolated [28]. Cyanobacteria strains often have a large number of Fdxs that act as electron donors in photosynthesis, oxidative and metal stress responses and in heterocyst specific metabolism [29–32]. While clearly being of physiological importance, the biochemical characterization of the Fdxs in cyanobacteria is still insufficient.

Fdxs have been suggested to be involved in Fe^{2+} release Bfr by direct protein-protein interaction [33]. Fdx from the pathogenic bacteria *Pseudomonas aeruginosa* has been shown to interact with, and reduce, the iron core of *Pa*Bfr *in vitro* as well as in the *P. aeruginosa* cell [34,35]. The interaction of Fdx and Bfr is thus established, but the protein-protein interactions that allow the reduction of the iron-core of Dps are still not known. Our intention with this study was to reveal if Fdxs interact with the two non-canonical Dps proteins of *N. punctiforme*. Despite the advancements in defining the roles of NpDps proteins in various cellular processes, many questions, especially concerning non-canonical Dps proteins, remain unanswered. The crystal structures of a number of Dps proteins have been resolved [13,25,36], but the biophysical structural diffusional properties of Dps proteins are still unknown. Here fluorescence correlation spectroscopy (FCS) and fluorescence resonance energy transfer (FRET) has been used to determine whether Dps proteins and Fdxs are interacting or not. In addition, we also explored the possible interaction with DNA, and the multimerization properties of NpDps4 and NpDps5 under various conditions.

2. Materials and methods

2.1. Bacterial strains, media and growth conditions

This research study was carried out with the heterocyst-forming cyanobacterium *Nostoc punctiforme* strain ATCC 29133-S (known as UCD 153) [37], *Escherichia coli* (*E. coli*) DH5α [38] and *E. coli* BL21(DE3) [39]. *E. coli* cells were grown aerobically at 37 °C and 200 rpm in LB (Luria - Bertani) medium. For solid media, 1.5% agar (Noble agar, BD, Difco, Franklin Lakes, NJ, USA) was used. 50 μg mL^{-1} ampicillin was used in solid and liquid LB media. Cyanobacteria were grown in BG11 [40] without the addition of $NaNO_3$, at 30 °C and 25–40 μmol photons m^{-2} s^{-1} in 100 mL *E*-flasks under shaking at 100 rpm, or in 250 mL–400 mL E-flasks under aeration and stirring. For solid media, 1% agar (Noble agar, BD, Difco, Franklin Lakes, NJ, USA) was used. Chlorophyll *a* measurements and light microscopy (Axiostar, ZEISS) on cultures were performed regularly. Cells were harvested by centrifugation and cell pellets were frozen in liquid nitrogen and stored at −80 °C, until further investigation.

2.2. Cloning of NpDps and NpFdx genes in pSBA13 vector

BioBrick plasmid pSB1A3 (http://parts.igem.org/Part:pSB1A3) was used for heterologous expression of NpDps and NpFdx proteins. A Strep (II)-tag (W-S-H-P-Q-F-E K) was linked *via* a short 2-alanine linker (GCC GCA) to the 3′ end of the targeted cloned gene, to which stop codon (TAA) was fused. The *E. coli* Dps protein-encoding gene, *P0ABT2* (*NC_000913.3*), *Npdps4 (Npun_R5799)*, *Npdps5 (Npun_F6212)* and the NpFdx protein-encoding genes, *Npfdx1 (Npun_F3727)*, *Npfdx9 (Npun_F4770)* and *NpfdxH* (*Npun_R0380*) were amplified from isolated genomic DNA of *E. coli* or *N. punctiforme*, and the genetic constructs were created using Overlap Extension (OE) PCR [41]. The vectors were transformed into *E. coli* DH5α [42]. The resulting verified correct constructs are listed in Table 1. Primers were designed using PrimerX software (http://bioinformatics.org/primerx/index.html) and are listed in Table 1.

2.3. Overexpression and purification of NpDps and NpFdx proteins

E. coli cells harboring pVM27, pVM28, pVM29, pVM30, and pVM31 (Table 1) were grown with additional $FeCl_3$ (0.1 g L^{-1}). Protein expression and purification were performed by IPTG induction and Streptactin chromatography as described by Howe et al. [43]. The elution of the Strep-tagged proteins was carried out in degassed equilibration buffer containing an additional 2.5 to 5 mM d-desthiobiotin (Sigma-Aldrich). To have semi-anaerobic conditions during purification. of NpFdx9, we used degassed buffers and oxygen scavenging enzymes, 8 U mL^{-1} glucose oxidase (Sigma-Aldrich) and 100 U mL^{-1} catalase (Sigma-Aldrich).

2.4. Non-denaturing and denaturing gel electrophoresis

Protein expression and purification were confirmed by Laemmli SDS-PAGE [44], as described [43]. To investigate the multimeric forms of the purified Dps proteins non-denaturing gel electrophoresis was performed as described by Howe et al. [43].

2.5. Sample preparation and mass spectrometry analysis

NpFdx, NpDps, and EcDps proteins were prepared and analyzed by MS as described by Howe et al. [43]. Protein sequences for NpFdx1, NpFdx9, NpFdxH, NpDps4, and NpDps5 were received from the Cyanobase database (http://genome.microbedb.jp/cyanobase/) [45] for *N. punctiforme* and NCBI protein databases (https://www.ncbi.nlm.nih.gov/protein/) for *E. coli*. Protein sequences were aligned using Clustal Omega [46].

Table 1
Plasmids and primers used in this work.

Plasmids	Relevant properties	
pSBA13	Strep-tagged, Amp^r	In this work
pVM27	*Npfdx1* cloned into pSBA13, Amp^r	In this work
pVM28	*Npfdx9* cloned into pSBA13, Amp^r	In this work
pVM29	*NpfdxH* cloned into pSBA13, Amp^r	In this work
pVM30	*Npdps4* cloned into pSBA13, Amp^r	In this work
pVM31	*Npdps5* cloned into pSBA13, Amp^r	In this work

Primers	Primer sequences (5′ to 3′)
Npfdx1_For	TACTCGAGAAAGAGGAGAAATACTAG ATGCCAACTTATAAAGTGACACTAATTAAC
Npfdx1_Rev	TTATTTTTCGAATTGGGGATGACTCCATGCGGC ATAGAGTTCTTCTTCTTTGTGA
Npfdx9_For	TACTCGAGAAAGAGGAGAAATACTAG GTGAAAAAACGAGTAACACTAACCTTC
Npfdx9_Rev	TTATTTTTCGAATTGGGGATGACTCCATGCGGC AAGGTTAGTGGAGATTGTA
NpfdxH_For	TACTCGAGAAAGAGGAGAAATACTAGATGG CTACCTACCAAGTTAGATTAATCAAC
NpfdxH_Rev	TTATTTTTCGAATTGGGGATGACTCCAT GCGGCTACGAGATATGCTTCTTGATGTG
Npdps4_For	TACTCGAGAAAGAGGAGAAATACTAGATGTCTGAAAGCGAAACTTTGTTACG
Npdps4_Rev	TTATTTTTCGAATTGGGGATGACTCCATGCGGCGCTTTGAGCCGCTTGGAC
Npdps5_For	TACTCGAGAAAGAGGAGAAATACTAGATGCAAGAACTTGACTATAAAAAGACTATC
Npdps5_Rev	TTATTTTTCGAATTGGGGATGACTCCATGCGGCGCTAAAATCGCGTAGCATCTTT
Ecdps_For	TACTCGAGAAAGAGGAGAAATACTAGATGAGTACCGCTAAATTAGTTAAATC
Ecdps_Rev	TTATTTTTCGAATTGGGGATGACTCCATTCGATGTTAGACTCGATAAACCACAGG
pSB1A3_For	CGTTCGGCTGCGGCGAGCGG
pSB1A3_Rev	GAGGCGGTTTGCGTATTGCTCTAGAAGCGG CCGCGAAT
pLac_For	GCCGCTTCTAGAGCAATACGCAAACCGCCT CTCCC
pLac_Rev	CTAGTATTTCTCCTCTTTCTCGAGTATGTGTGAA ATTGTTATCCGCTCAC
Term_For	GGAGTCATCCCCAATTCGAAAAATAACCAGGC ATCAAATAAAACGAAAGGC
Term_Rev	GCTCACTCAAAGGCGGTAAT

2.6. Electrophoretic mobility shift assay (EMSA)

Prior to gel electrophoresis, 125 ng of pSB1A3 plasmid DNA (2.5 kbp) was mixed with 1 μg of each of the purified proteins at pH 6.0 and pH 7.0 in 5 μL MES and Bis-Tris buffer systems (50 mM NaCl and 100 mM buffer), respectively. After a 15 min incubation step at 22 °C, 1 μL of 6 x loading buffer (60% (v/v) glycerol, 50 mM NaCl and 0.1% (w/v) bromophenol blue) was added. The reaction volume was applied to a 1% (w/v) agarose gel (50 mM NaCl and 10 mM of MES or Bis-Tris buffer). Gel electrophoresis was performed at a voltage of 30 V for 45 min at 22 °C. The gels were stained in thiazole orange containing MES running buffer for 1 h under shaking in darkness. After two washing steps with demineralized water, documentation was performed on a Chemi Doc XRS (Bio-Rad). 1 μg of *E. coli* Dps, EcDps, and 1 μg bovine serum albumin (BSA) (Sigma) served as positive and negative controls respectively.

2.7. Dynamic light scattering (DLS)

Purified NpDps and EcDps proteins were diluted to a concentration between 70 and 100 μg mL^{-1} into 50 mM NaCl and 100 mM buffer containing HEPES (pH 3.0), acetate (pH 5.0), succinate (pH 6.0), phosphate (pH 7.0), Tris (pH 8.0) and Bis-Tris propane (pH 9.0). All buffer components were individually filtered (0.45 μm Millipore filter HAWP-AO, Merck) before mixing. Prior to DLS analysis, all samples were centrifuged at 13,000 × *g* for 5 min at 22 °C. DLS analysis was performed at 173° (backscattering) on a Zetasizer Nano instrument (Malvern) using 1 cm path length polystyrene cuvettes (VWR). Experiments were performed at 25 °C. At each pH, 5 to 13 data sets (each 100 s in duration) were collected for each protein. The hydrodynamic diameter of each protein species was calculated based on the mean from each dataset (number related size distribution). For background measurements, five datasets (each 100 s in duration) were collected for solutions at each pH without protein.

2.8. UV–visible spectrophotometry and EPR spectroscopy of NpFdx proteins

UV–visible spectra of NpFdx1, NpFdxH, and NpFdx9 in their as-isolated state were measured either in 1 mL quartz cuvettes or in EPR quartz tubes (0.3 cm path length) in a Varian Cary 50 Bio UV–visible spectrophotometer. Samples were diluted with 100 mM Tris-HCl pH 8.0 + 150 mM NaCl buffer when necessary so as to keep Abs < 1 for relevant features in the visible region of the spectra. For electron paramagnetic resonance (EPR) spectroscopy, 150–200 μL of each sample in the as-isolated state was introduced in EPR quartz tubes suitable for X-band experiments. The tubes were then flushed with argon, capped with rubber septa, and frozen and kept in liquid nitrogen (77 K) storage until measurement. Spectra were acquired at cryogenic temperatures (T = 7 to 20 K) using liquid helium as a coolant in a Bruker ELEXYS E500 spectrometer using an ER049X SuperX microwave bridge, and a Bruker SHQ4122 cavity, equipped with an Oxford Instruments continuous flow cryostat, and using an ITC 503 temperature controller (Oxford Instruments). To analyze the reduced state of iron-sulfur clusters in all ferredoxins, sodium dithionite (Sigma-Aldrich) was added to each EPR sample to a final concentration of 5 mM (from a freshly-prepared anaerobic 100 mM stock solution in 100 mM Tris-HCl pH 8.0 + 150 mM NaCl buffer). After incubation at room temperature (20 °C) for 30 min, samples were re-frozen and new spectra were

acquired. Spin quantification was performed based on the concentration of protein as calculated from UV–visible spectra, assuming $\varepsilon_{420} = 9500\ M^{-1}\ cm^{-1}$ for both NpFdx1 (100 μM) and FdxH (185 μM) and $\varepsilon_{420} = 15{,}000\ M^{-1}\ cm^{-1}$ for Fdx9 (33 μM), and using 1 mM $CuSO_4$ in 10 mM HCl as spin standard. Spectra acquisition and analysis were performed using the Xepr software package (Bruker).

2.9. Protein labeling and sample preparation

In Fluorescence correlation spectroscopy (FCS) experiments, lysines of NpDps and cysteines of NpFdx proteins were labeled with the fluorophore Atto550 (λex 544 nm; λem 576 nm) by following the protocol provided by the manufacturer (Atto-Tec) respectively. For DNA binding experiments, linear DNA was used in all experiments. In Fluorescence resonance energy transfer (FRET) experiments, lysines were labeled with donor Atto550 and cysteines were labeled with acceptor Atto647N (λex 644 nm; λem 661 nm) in NpDps and NpFdx proteins, respectively. In all cases, excess fluorophore was added to the aqueous protein solution and left for 8 h at 4 °C. The labeled protein was subsequently purified using size exclusion chromatography on a Sephadex™ G-25 Medium column (GE Healthcare, UK). To remove excess free dyes from the labeled proteins and also avoid hydrolysis of an extra fluorophore, the samples were dialyzed (3 k membrane) two times, 4 h of incubation in each time at 4 °C. The freshly prepared complexes were immediately used for FCS and FRET experiments. For DNA and NpDps proteins interaction study, linear dsDNA (~0.25 kbp, 500 nM) 5′GCTCTAGACCGGCCGTTCTAGCTATTCGCATAACCATGCAGAATTTCTCGATCGCCGTACCTCTACACCGTATCATGACATTAACCTATAATAGGCGTATCACGAGGCAGAACAAAGTAATACTCATTGCGACTTCTTAATTCGATATATTAGTCAAATAGGGGTTCCGCGCACATTTCCCCGAAAAGTGCCACCTGACGTCTAAGAAACCTAAGAAAGCGCAAGGAACGTTTACGGCCGCTTGGGAATTCCGAC3′, was incubated 30 min at 22 °C with 50 nM of the each purified and labeled NpDps using 50 mM Bis-Tris and HEPES buffer systems supplemented with 150 mM NaCl at pH 6.0 and pH 8.0 respectively. In the case of FCS experiments considering NpFdxs interactions with NpDps, 100 nM of each labeled NpFdxs were mixed with 500 nM of each unlabeled NpDps for 2 h at pH 6.0 and 8.0. In the case of FRET experiments, 10 nM of each labeled NpDps were mixed with 50 nM of each labeled NpFdxs using 50 mM Bis-Tris buffer supplemented with 150 mM NaCl at pH 6.0. In all cases, we added 0.1% Tween-20 (Sigma) to the samples in order to diminish surface interactions with the glass coverslip.

2.10. Fluorescence correlation spectroscopy

FCS experiments were carried out with a custom-built confocal fluorescence microscope with a Zeiss C-Apochromat 40 × 1.2NA H_2O-immersion objective at 22 °C. The fluorescence intensity temporal fluctuations were analyzed with a hardware correlator (Flex02-12D/C correlator). All the experimental data were fitted in considering a single species and free Brownian 3D diffusion in the case of a Gaussian molecular detection efficiency.

$$g^{(2)}(\tau) = 1 + \frac{1}{N}\left(1 - \frac{B}{F}\right)^2 \cdot \left(1 + n_T \cdot exp\left(-\frac{\tau}{\tau_T}\right)\right) \cdot \frac{1}{\left(1 + \frac{\tau}{\tau_d}\right)\sqrt{1 + s^2\left(\frac{\tau}{\tau_d}\right)}} \quad (1)$$

where N is the average number of molecules in the focal volume, F is the total fluorescence signal, B is the background noise, n_T is the amplitude of the dark state population, τ_T is the dark state blinking time, τ_d is the mean diffusion time and S is the ratio of transversal to axial dimensions of the analysis volume. The molecular diffusion coefficient, D and hydrodynamic radius, R_H were calculated as previously as described in detail [47]. The confocal volume was defined by using the 30 μm confocal pinhole conjugated to the sample plane whose transversal waist w_{xy} was calibrated to 285 nm using the known diffusion coefficient of Alexa 647 in pure water ($3.1 \times 10^{-6}\ cm^2 \cdot s^{-1}$ at 22 °C) and known hydrodynamic radius of 0.7 nm in pure water.

2.11. Fluorescence resonance energy transfer (FRET)

FRET detection was performed on a confocal inverted microscope with a Zeiss C-Apochromat 63 × 1.2NA water-immersion objective, and an iChrome-TVIS laser (Toptica GmbH) as an exciting source operating at 550 nm. The excitation power at the diffraction-limited spot was set to 20 μW for all experimental conditions. Filtering the laser excitation was achieved by a set of two band-pass filters (Chroma ET525/70M and Semrock FF01-550/88). Dichroic mirrors (Chroma ZT594RDC and ZT633RDC) separate the donor and acceptor fluorescence light. The photodiode signal was recorded by a fast time-correlated single photon counting module (Hydraharp400, Picoquant GmbH) in time-tagged time-resolved (TTTR) mode. The detection was performed by two avalanche photodiodes (Micro Photon Devices MPD-5CTC with 50 μm active surface) with 620 ± 20 nm (Chroma ET605/70 M and ET632/60 M) and 670 ± 20 nm (Semrock FF01-676/37) fluorescence band-pass filters for the donor and acceptor channels respectively. All fluorescence bursts above the background noise were recorded separately by the acceptor channel and donor channel. As a part of calibration, we took into consideration differences in the fluorescence detection efficiencies (η_A and η_D), direct excitation of the acceptor by the laser light ($n_A{}^{de}$), donor emission crosstalk into the acceptor channel (α) and quantum yields of fluorophores (φ_A and φ_D). Symphotime 64 (Picoquant GmbH) software was used to compute the FRET efficiency according to the formula below:

$$E = \frac{n_A - \alpha n_D - n_A^{de}}{n_A - \alpha n_D - n_A^{de} + \gamma n_D} \quad (2)$$

where $\gamma = \eta_A\varphi_A/\eta_D\ \varphi_D$ accounts for the differences in quantum yields (φ_A and φ_D) and fluorescence detection efficiencies (η_A and η_D) between the acceptor and donor.

We estimate $\gamma = 1.3$, and $\alpha = 0.16$ for the current setup. The Förster distance between the selected FRET pair is 62.6 Å.

3. Results

3.1. Screening for ferredoxin candidates in Nostoc punctiforme

To identify ferredoxin (NpFdxs) candidates to be used in the NpDps-Fdx interaction studies, we conducted *in silico* analysis of all annotated Fdxs in *N. punctiforme* (Table S1, Figs. S1 and S2). The Fdx, PaBfd from *Pseudomonas aeruginosa* (Figs. S1 and S2) was chosen as a template for the investigation, since this protein has shown to interact with the Bfr from *P. aeruginosa* [35], and is involved in iron reduction and release from the Bfr. The phylogenetic study revealed one clade of [2Fe-2S]-cluster Fdxs, consisting of PaBfd and six NpFdxs, and one clade consisting of seven [4Fe-4S]-cluster NpFdxs (Figs. S1 and S2). Among these, we proceeded with (i) NpFdx1, a homologue of a well-studied Fdx involved in photosynthesis in the cyanobacterium *Synechocystis* PCC 6803 [30], (ii) NpFdxH, which homologue in *Anabaena variabilis* is heterocyst-specific [32], and (iii) NpFdx9 (Npun_F4770), which homologue in *Synechocystis* PCC 6803 is involved in oxidative and metal stress [30]. As the [Fe—S] cluster unit of the Fdx protein determines its cellular activities [48], we selected both [2Fe-2S] and [4Fe—4S] center-containing ferredoxins for the studies of interaction with NpDps4 and NpDps5.

3.2. Purification and SDS-PAGE analysis of NpDps and NpFdx proteins

All NpDps and NpFdx proteins, except NpFdx9, which contains the O_2-sensitive [4Fe—4S] cluster, were purified using aerobic conditions. For NpFdx9 purification, we used partial anaerobic conditions, with de-

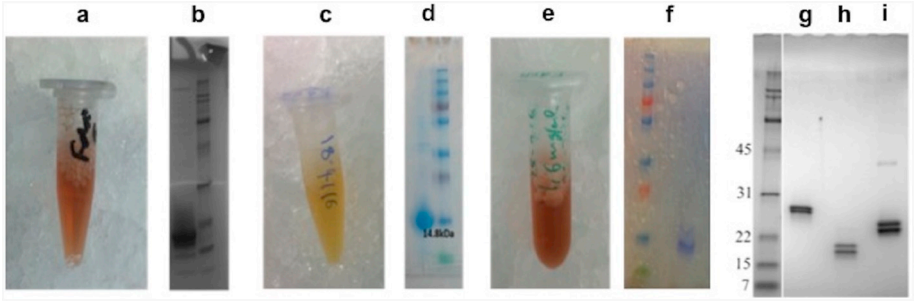

Fig. 1. SDS–PAGE analysis of the recombinantly expressed and purified NpFdx, NpDps and EcDps. The calculated molecular mass of the proteins includes the added 2-alanine linker and Strep(II)-tag. The red colored ([2Fe−2S] cluster) NpFdx1 (a), and NpFdxH (e), and orange colored ([4Fe−4S] cluster) NpFdx9 (c) are shown. Panels b, d and f are showing protein bands of NpFdx1, NpFdx7, and NpFdx9 with calculated molecular sizes of 11.8 kDa, 12 kDa and 15.8 kDa respectively. Panels g, h and i are showing protein bands of NpDps4, NpDps5 and EcDps with calculated molecular sizes of 22.0 kDa, 17.7 kDa and 19.9 kDa respectively. SDS-PAGE Broad Range Molecular weight standards (Bio-Rad) were used as molecular mass markers. Gels were stained with colloidal Coomassie dye. 1 μg of each of the purified proteins was loaded on a SDS-PAGE gel. The identities of the protein within each protein band were confirmed by mass spectrometry [50].

gassed buffers, containing oxygen-scavenging enzymes. The purity of the proteins NpFdx1, NpFdx9, NpFdxH, NpDps4, and NpDps5, were analyzed by SDS-PAGE (Fig. 1). This analysis resulted in protein bands corresponding approximately to the theoretical sizes of the proteins including the attached Strep(II)- tag (Fig. 1). Mass spectrometry (MS) analysis of NpFdx protein bands confirmed their identity as respective NpFdx protein. For NpDps proteins, a 22 kDa protein size band was observed for NpDps4 (Fig. 1g) and two ~ 20 kDa bands for NpDps5 (Fig. 1h). All protein bands were analyzed and confirmed by MS. The origin of the double band pattern for NpDps5 is unknown. For EcDps, two strong protein size bands at ~22 kDa and a faint 37 kDa protein size band were observed (Fig. 1i). MS analysis identified all three bands as EcDps sequences and a similar band pattern has been observed earlier in SDS-PAGE [49]. Schmidt et al. [49] identified the double band pattern as being a result of N-terminal digestion. The EcDps protein band of 37 kDa might be a Dps-dimer as it was also identified by MS to be EcDps.

3.3. Spectroscopic characterization of NpFdxs

To ensure that the isolated NpFdx contained intact iron-sulfur clusters, and thus may act as electron donors to the NpDps, the number of iron and sulfur atoms of the iron-sulfur centers in the purified NpFdx samples were analyzed by UV–visible absorption spectroscopy in their as-isolated states. Furthermore, due to the lack of biochemical data about the NpFdx, this examination was also conducted to verify the annotations of Fe—S clusters for NpFdx1, NpFdx9, and NpFdxH. Even though these Fdxs are annotated as [2Fe-2S] or [4Fe—4S] proteins, there have not been any experimental evidence established so far. This novel spectral information was crucial to proceed further with the biochemical and biophysical experiments. NpFdx1 exhibited well-defined absorption bands in the near-UV and visible regions with maxima at 277, 331, 421 and 464 nm (Fig. S6b, upper panel). NpFdxH showed a very similar spectrum, with maxima at 278, 334, 422 and 469 nm (Fig. S6b, middle panel). These spectral characteristics arise from ligand-to-metal charge transfer bands that are typical for [2Fe—2S] centers in the oxidized state [51]. In contrast, NpFdx9 presented broader absorption bands around the 320 and 420 nm region characteristic of proteins containing [3Fe—4S] and/or [4Fe—4S] centers (Fig. S6b, lower panel) [51]. In order to know the state of intact and functional features of [Fe-S] centers in the purified NpFdx proteins, EPR spectroscopy studies were conducted in their as-isolated, and chemically reduced states, using continuous wave X-band electron paramagnetic resonance at cryogenic temperatures. In its as-isolated state, no resonances were visible for NpFdx1 (not shown) between $T = 11$ K and $T = 20$ K; this result is consistent with the presence of [2Fe-2S] centers in the oxidized state. Upon one-electron reduction, a low-spin signal (S = 1/2) was clearly detectable at $T = 15$ K (Fig. S6a, upper panel). The spectrum presented a rhombic-shaped signal with field components at $g_x = 1.90$, $g_y = 1.97$ and $g_z = 2.06$, and is characteristic for reduced [2Fe—2S] centers [58]. Spin quantification yielded 0.93 spin/metal center, very close to the expected 1 spin/center. The same analysis was applied to NpFdxH. In the as-isolated state, NpFdxH did not show any signals in EPR spectroscopy (not shown), but upon reduction, a low-spin signal (S = 1/2), was clearly detectable at T = 15 K (Fig. S6a, middle panel). The spectrum shows field components at $g_x = 1.92$, $g_y = 1.96$ and $g_z = 2.05$; relaxation properties (not shown) are consistent with the presence of [2Fe-2S] centers. Spin quantification yielded 0.82 spin/metal center, which is slightly lower than NpFdx1; the difference might be due to incomplete reduction. In its as-isolated state. NpFdx9 exhibited a narrow signal centered at around $g = 2.02$ at $T = 7$ K (Fig. S6a, lower panel). Temperature and applied microwave power saturation behavior (not shown), as well as signal shape and field position, are characteristic of a low-spin, S = 1/2 [3Fe—4S] cluster in the oxidized state; [4Fe—4S] centers are EPR-silent (S = 0) in the oxidized state [57]. Spectra acquired after reduction show the presence of mixed low-spin, S = 1/2 species at $T = 11$ K characteristic of [4Fe-4S] centers (Fig. S6A, lower panel) [51]. The heterogeneity of the spectrum suggests the presence of mixed populations of protein presenting different spin distributions. Nevertheless, resonance shape and field positions, as well as temperature and applied microwave power saturation (not shown), indicate that the signals arise from magnetically uncoupled [4Fe—4S] centers. Spin quantification in NpFdx9 allowed us to estimate that most (0.80 spin/metal center) of EPR-detectable iron-sulfur centers were [4Fe—4S] centers, with a minor population (~20%) being [3Fe—4S] centers. The presence of [3Fe-4S] centers is most likely due to the fact that the protein was purified in semi-anaerobic conditions, which can lead to the (reversible) loss of one iron.

3.4. Multimerization properties of NpDps proteins

The iron storage ability of Dps proteins is dependent on the oligomerization state of the protein complex. Therefore, we determined the state of the purified NpDps4 and NpDps5, under the different pH conditions that were used in the NpDps-NpFdx interaction investigations.

To find the native multimeric sizes of the NpDps proteins, we used four different strategies (i) non-denaturing polyacrylamide gel electrophoresis (PAGE), (ii) size exclusion chromatography (iii) dynamic light scattering (DLS) and (iv) fluorescence correlation spectroscopy (FCS). Both NpDps4 and NpDps5 showed multimeric protein complexes when analyzed with non-denaturing PAGE at an approximate pH of 8.0 (Fig. 2a). Both NpDps4 and NpDps5 proteins formed large protein complexes, similar in sizes to the control protein EcDps that shows one clear band on the gel corresponding to the dodecameric form of the protein. NpDps5 also showed a band corresponding to a protein complex of lower mass. The approximate molecular masses of each NpDps protein were based on using the different multimeric forms of bovine serum albumin (BSA) as marker proteins [52], (Fig. 2a). To investigate the oligomeric forms and stability of NpDps4 and NpDps5, we performed DLS experiments under different pH conditions, ranging from pH 3.0 to pH 9.0 (Fig. 2b). EcDps served as a control protein to indicate the size of a Dps dodecamer, which has been earlier reported to be

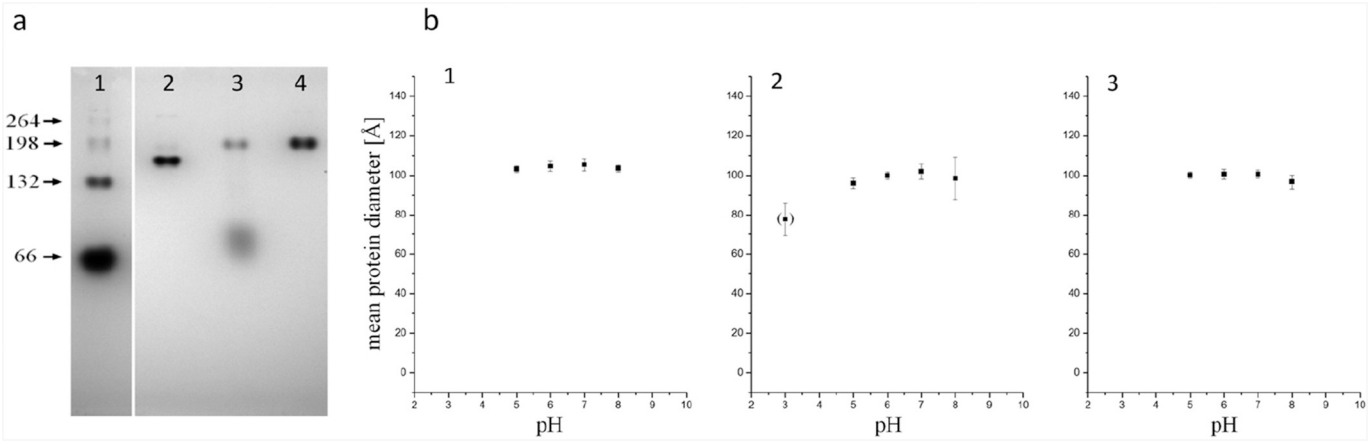

Fig. 2. Multimeric size of the NpDps4, NpDps5, and EcDps analyzed by non-denaturing PAGE and Dynamic light scattering (DLS). Non-denaturing PAGE (a) shows theoretical molecular masses of putative dodecamers were 262 kDa for NpDps4 (a1), 210 kDa for NpDps5 (a2), and 236 kDa (a3) for EcDps. Additionally, the different native forms of bovine serum albumin (BSA) were used for estimating the approximate molecular masses. The pH of the gel was 8.45 and the pH of the running buffer was 8.0. Dynamic light scattering (b) shows the hydrodynamic diameters of NpDps4 (b1), NpDps5 (b2) and EcDps (b3) proteins at different pH. All protein species are displayed as a mean of the average hydrodynamic diameter from each experimental series in (Å) at pH 3.0, 5.0, 6.0, 7.0 and 8.0. Particles with a lower peak occurrence than 1% (number related) are not shown, whereas particles with occurrence between 1% and 10% are shown in brackets. Standard error of the mean particle diameters is given as error bars.

~101 Å in hydrodynamic diameter by DLS analysis [53]. The monomeric form of EcDps derived from the crystal structure, possesses a cylindrical shape with its dimensions of about 17 × 60 Å (radius × height) not including the random coil of the N- and C-termini (PDB:1DPS). At a pH range between 5 and 8, NpDps4, NpDps5 and EcDps formed protein species with an average hydrodynamic diameter larger than 99 Å indicating the presence of multimeric protein complexes, presumably dodecamers. It should be noted that the standard error of the multimer of NpDps5 at pH 8.0 is comparatively large and may indicate a partial decomposition. At pH 3.0, NpDps5 was occasionally observed to form a protein species with a hydrodynamic diameter of 78 Å, indicating dissociation to a lower stable multimeric state, and at pH 9.0 no protein species were found for any of the Dps, which may be due to complete protein denaturation. We also determined the overall oligomerization state of NpDps4 and NpDps5 in solution, by using size-exclusion chromatography, at pH 6.0 and 8.0. EcDps was used as a control. NpDps4 showed one well-defined oligomerization state at both pH 6.0 and pH 8.0. NpDps5 on the other hand showed one high multimeric conformation, but also one lower multimeric state at both pH 6.0 and 8.0 (Fig. S3). The well-characterized *E. coli* Dps showed one high multimeric state at approximately the same retention time as the high multimeric states of both NpDps4 and NpDps5, thus indicating that all these Dps proteins are, in solution, at least partially, in a dodecameric form.

To explore the multimerization states of NpDps4 and NpDps5, the effect of global free diffusion of both NpDps proteins in aqueous solution were measured by FCS. Both NpDps4 and NpDps5 show the monophasic autocorrelation curves with diffusion times of 780 ± 20 µs ($D = 2.11 \times 10^{-7}$ cm^2·s^{-1}) and 740 ± 16 µs ($D = 2.24 \times 10^{-7}$ cm^2·s^{-1}) in aqueous solution at pH 6.0, respectively (Fig. 3c and d, Table S2). The calculated hydrodynamic radii of the NpDps4 were ≈10.7 nm and ≈11 nm at pH 6.0 and pH 8.0 respectively (Fig. 3e). In sharp contrast, at pH 8.0, NpDps5 showed reduced diffusion times and decreased hydrodynamic radii around ≈5.61 nm ($D = 4.04 \times 10^{-7}$ cm^2·s^{-1}) (Table S3) as compared to 10.1 nm ($D = 2.24 \times 10^{-7}$ cm^2·s^{-1}) at pH 6.0 (Fig. 3d and f, Table S2). In all the FCS experiments, we considered triplet state populations were < 10%.

3.5. DNA binding properties of NpDps

Dps are known to mechanically protect the genetic material of some bacteria against oxidative stress, in part due to the ability to bind to DNA [54]. To investigate the DNA binding properties of the two atypical NpDps, and to resolve if these were dependent on the pH and multimeric state of the NpDps, we conducted both in-solution as well as in-gel studies. In electrophoretic mobility shift assay (EMSA) both NpDps4 and NpDps5 formed dsDNA-Dps complexes at pH 6.0 as indicated by the DNA retardation in the gel (Fig. 3a). It is noticeable that NpDps4 shows weaker dsDNA-binding affinity than NpDps5 at pH 6.0 (Fig. 3a). At pH 7.0 the dsDNA-binding affinity for both NpDps was completely abolished (Fig. 3b). In neither pH condition the complete amount of the dsDNA was bound by the NpDps (unbound dsDNA was still observed) (Fig. 3a and b). We further studied the diffusion time of labeled NpDps upon interaction with dsDNA by using FCS, and the results showed that in solution both NpDps4 and NpDps5 show interaction with dsDNA at pH 6.0 (Fig. 3c and d). In case of NpDps4, the diffusion times are longer, in the range of 960–1020 µs ($D = 1.71–1.62 \times 10^{-7}$ cm^2·s^{-1}) in the presence of dsDNA molecules in comparison with the NpDps4 alone at both pH 6.0 and pH 8.0 (Fig. 3c). The calculated hydrodynamic radii increased from ≈10.1 nm to ≈13.2 nm and ≈14.0 nm when the Npdps4 were incubated with dsDNA at both pH 6.0 and pH 8.0 (Fig. 3e). NpDps5 shows a similar increase in the calculated hydrodynamic radii from ≈10.1 nm to ≈13.4 nm in the presence of dsDNA at pH 6.0 (Fig. 3f). On another hand, NpDps5 showed a similar range of diffusion times, and corresponding hydrodynamic radii ranges from ≈5.6 nm to ≈4.5 nm in the presence (respectively absence) of dsDNA at pH 8.0 (Fig. 3f). Thus, the FCS results clearly supported the in-gel (EMSA) results and showed that both NpDps4 and NpDps5 interact with DNA.

3.6. NpDps-NpFdx interactions

To investigate the possible interactions between NpDps and NpFdx proteins, and how this interaction may change depending on pH, FCS studies were conducted. To determine the hydrodynamic radii of NpFdx1, NpFdx9 and NpFdxH, and how the corresponding hydrodynamic radii modulate upon interaction with NpDps, we measured the diffusion times of labeled NpFdx with or without excessive amounts of NpDps4 or NpDps5 proteins. All free labeled NpFdx proteins show similar diffusion times of 300 ± 20 µs ($D = 5.4 \times 10^{-7}$ cm^2·s^{-1}) at both pH 6.0 (Fig. S4) and pH 8.0 (data not shown). In the presence of NpDps4, all the NpFdx proteins showed increased diffusion time of 760 ± 30 µs ($D = 2.1 \times 10^{-7}$ cm^2·s^{-1}), as compared to only the isolated NpFdxs, at both pH 6.0 and 8.0 as

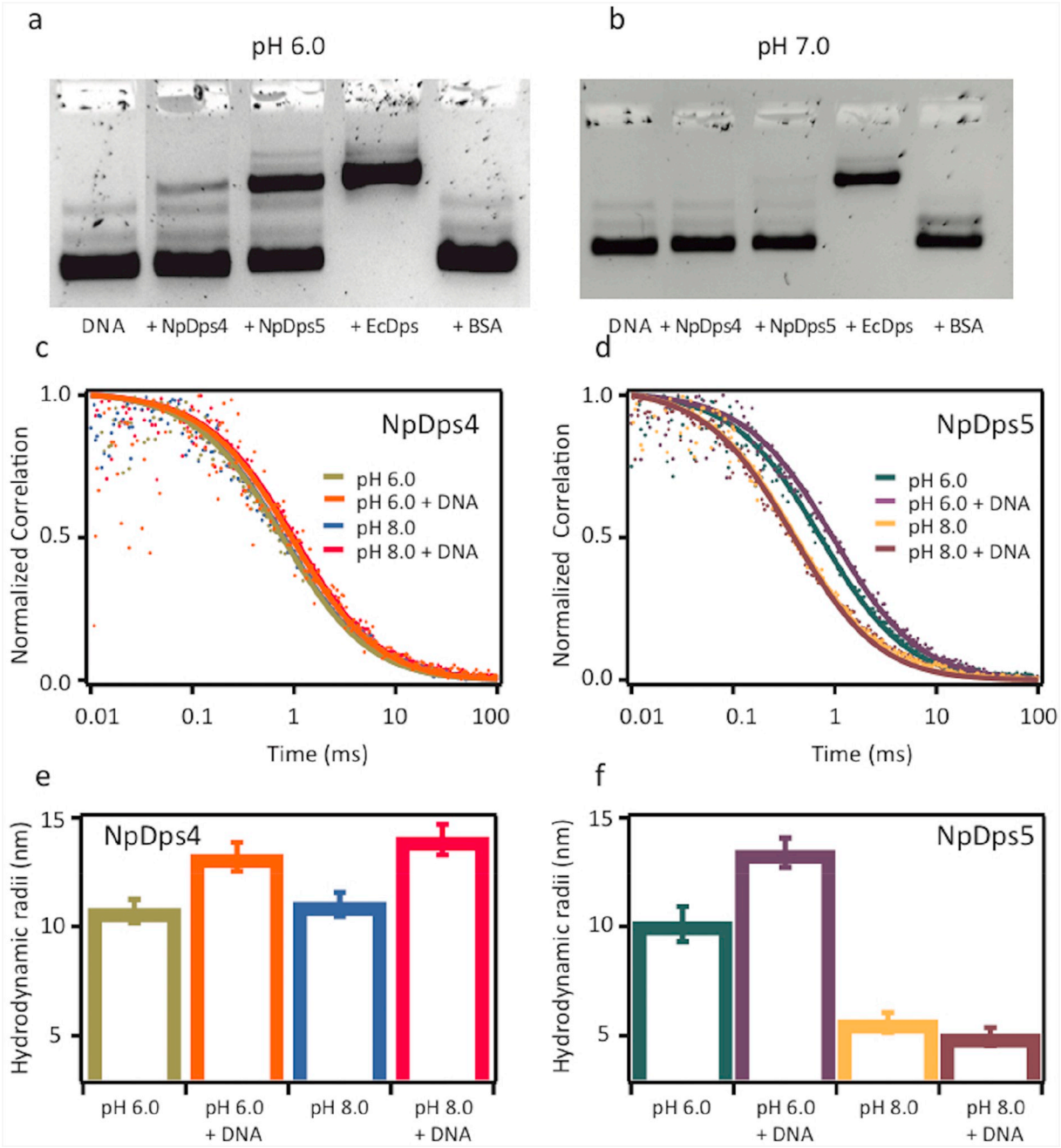

Fig. 3. DNA binding properties of fluorescence labeled NpDps4, NpDps5 and unlabeled EcDps at different pH using EMSA and FCS methods. EMSA analysis of the DNA binding properties of the NpDps proteins at pH 6.0 (a) and pH 7.0 (b). 125 ng of plasmid DNA (pSB1A3 vector) was incubated with 1 μg of NpDps protein material and separated on an agarose gel (1%). EcDps and BSA served as positive and negative controls respectively. Plasmid DNA is shown in lane "DNA". Thiazole orange staining was performed after gel electrophoresis for DNA detection. Normalized FCS correlation traces of NpDps4 (c), NpDps5 (d) and corresponding apparent hydrodynamic radii (e & f) obtained in the absence or presence of unlabeled dsDNA at pH 6.0 and at pH 8.0 in aqueous solution. Both NpDps4 and NpDps5 proteins show the monophasic autocorrelation curves.

exemplified for NpFdx1 (Fig. 4a). The calculated hydrodynamic radii result from the FCS data, summarizes that NpDps4 induce a similar noticeable change in hydrodynamic radii of NpFdx1, NpFdx9, and NpFdxH upon interactions at both pH 6.0 and 8.0 (Figs. 4c and S5). In the presence of NpDps5, NpFdx1, NpFdx9 and NpFdxH showed increased diffusion times of 810 ± 20 μs ($D = 2.0 \times 10^{-7}$ cm^2·s^{-1}), 780 ± 20 μs ($D = 2.1 \times 10^{-7}$ cm^2·s^{-1}) and 660 ± 20 μs ($D = 2.4 \times 10^{-7}$ cm^2·s^{-1}) respectively, as compared to only the isolated NpFdxs (Fig. S5). The calculated hydrodynamic radii of NpDps5 in interaction with NpFdx1, NpFdx9 and NpFdxH were 11.1 nm, 10.6 nm, and 9.0 nm at pH 6.0 (Fig. 4c, Fig. S5, and Table S2). At pH 8.0, NpFdx1, NpFdx9, and NpFdxH in the presence of NpDps5 show diffusion times of 430 ± 30 μs ($D = 3.8 \times 10^{-7}$ cm^2·s^{-1}), 450 ± 20 μs ($D = 3.7 \times 10^{-7}$ cm^2·s^{-1}) and 309 ± 10 μs ($D = 5.3 \times 10^{-7}$ cm^2·s^{-1}) (Fig. S5). The calculated hydrodynamic radii of NpDps5 in interaction with NpFdx1, NpFdx9 and NpFdxH at pH 8.0 were 5.8 nm, 6.1 nm, and 4.2 nm respectively (Fig. 4c, Fig. S5, and Table S3) indicating weak interactions at pH 8.0.

Based on the present data, we may conclude that under these experimental conditions both the NpDps4 and NpDps5 were multimers, putative dodecamers, at pH 6.0. At this pH similar hydrodynamic radii were identified for NpFdx1 and NpFdx9 upon interactions with both NpDps4 and NpDps5. These results were similar when the labeled

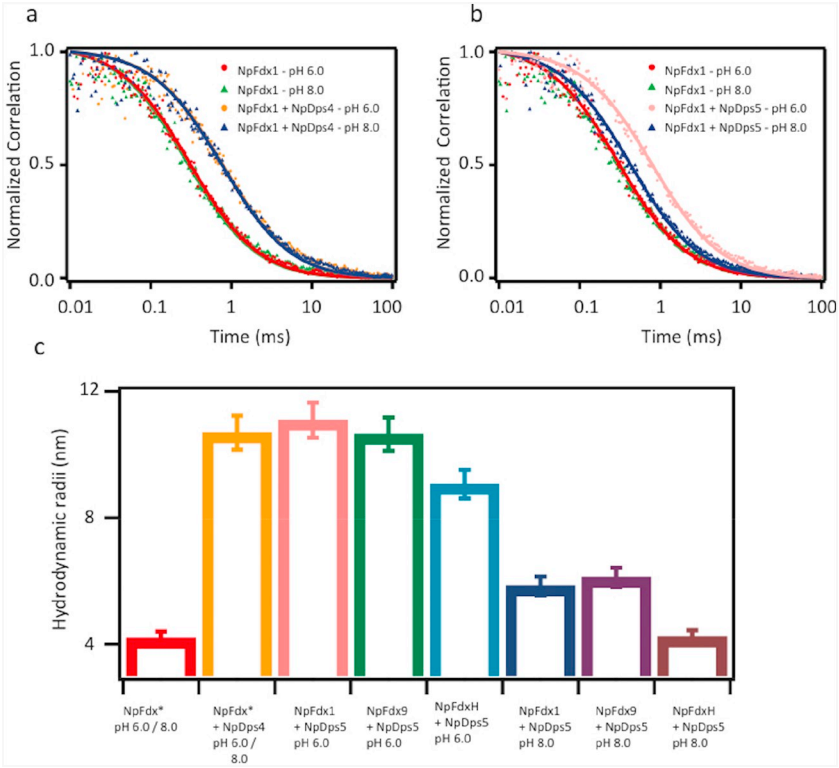

Fig. 4. FCS data on the labeled NpFdxs in concern together with excess amounts of NpDps4 and NpDps5 in aqueous solution. Normalized FCS correlation traces of NpFdx1 in the presence of NpDps4 (a) and in the presence of NpDps5 (b) at pH 6.0 and 8.0 in aqueous solution. Deduced hydrodynamic radii obtained for ferredoxin proteins (NpFdx*) in the absence or presence of NpDps4 and NpDps5 at pH 6.0 and 8.0 (c). Here, NpFdx* represents NpFdx1/NpFdx9/NpFdxH. For details see Supporting Fig. 5.

NpFdx protein concentrations were kept at a constant concentration of 100 nM and a high concentration of unlabeled NpDps (2 μM) were added. Thus, the results indicate that even at high concentrations of proteins, it seems very likely, that the formed NpDps multimeric complexes stay in a stable soluble multimeric form in aqueous solution at pH 6.0. At more basic conditions NpDps5 does not occur to be a stable dodecamer, which is reflected in the determined lower hydrodynamic radii of all NpFdx upon interaction with NpDps5 at pH 8.0 in comparison with at pH 6.0 (Fig. 4c and Fig. S5).

To determine possible interactions of NpFdxs and NpDps we used a confocal single molecule fluorescence resonance energy transfer strategy (FRET). By this method we determined if two fluorophores, in this case labeled NpFdxs and labeled NpDps are within a certain distance of each other. FRET histograms of the labeled NpFdxs in the presence or absence of labeled NpDps, at pH 6.0, are summarized in Fig. 5. A pH of 6 was used to ensure the NpDps were in their multimeric states. For all of the only donor labeled NpFdxs that are freely diffusing in solution only one peak was observed in the energy transfer efficiency (E) histograms, as exemplified for NpFdx1 (Fig. 5a). In the following description of the results, the normalized FRET values were interpreted, as a binding efficiency between NpDps and NpFdx proteins, would be visible as a change of FRET value. NpFdx1-NpDps4 interaction gave an maxima $E \sim 25\%$ (Fig. 5a). NpFdxH-NpDps4 interaction shows a similar $E \sim 31\%$ (Fig. 5c), while the NpFdx9-NpDps4 interaction shows a higher energy transfer efficiency maxima $E \sim 58\%$ (Fig. 5b). Thus, indicating that the average distance between the labeled NpDps4 and labeled NpFdx9 are smaller as compared to the average distance between NpDps4 and NpFdx1 or NpFdxH. The interaction of NpDps5 as compared to the interaction of NpDps4 with the three NpFdx showed a different pattern of energy transfer efficiency maxima. The interaction of NpDps5 with NpFdx1 and NpFdx9 gave similar E of ~63% and ~56%, respectively (Fig. 5d and e), while the NpDps5-FdxH interaction shows a clear left-shifted peak at E ~ 15% (Fig. 5f), which suggests that the average distance between NpDps5 and NpFdxH are longer as compared to the average distance between NpFdx1/NpFdx9 and NpDps5.

4. Discussion

Here we continue our exploration of ferritin-like proteins in *N. punctiforme*, which is a bacterium, equipped with an unusually complex set of five Dps proteins (NpDps1 – 5). In our earlier studies, NpDps1 - 3 were shown to cluster together with Dps proteins, such as the Dps family prototype of *Escherichia coli*, and thus classified as canonical Dps proteins. On the other hand, NpDps4 were clustered with atypical Dps, and NpDps5 with Bfrs, and were therefore classified as non-canonical Dps proteins [20,43]. Our working hypothesis is that each NpDps protein has a specific physiological role, and insights into their biochemical properties will help to understand the multilayered network of iron homeostasis and oxidative stress tolerance in *N. punctiforme*. In this study we hypothesized that NpFdx interact with the two atypical Dps proteins in *N. punctiforme*, and therefore may mediate electron transfer for reduction and release of the stored iron.

We also aimed at describing NpDps4 and NpDps5 in terms of their protein multimerization, pH stability and their possible interaction with ferredoxins and DNA. Indeed, the results obtained from the interaction studies of NpDps and NpFdxs show for the first time that Dps proteins can interact with Fdxs. Although the physiological relevance of the NpDps-NpFdx interaction is hard to predict, our results show that the interactions are dependent on pH, state of multimerization of the Dps and on the specific NpDps-NpFdx pair.

4.1. NpDps4 and NpDps5 form dodecameric structures

For the Dps to be able to store iron within the cell it needs to be in its multimeric form under physiological conditions. Certainly, both NpDps4 and NpDps5 form high states of multimeric complexes, presumably dodecamers under physiological pH. Recent crystal structure data support this and revealed that NpDps4 forms a dodecameric hollow sphere [25]. Of the two, NpDps4 was found to be more stable within a wider range of pH conditions. The level of multimerization was similar for the two NpDps, which suggest that even if NpDps5 is structural similar to a Bfr [20] it forms a dodecameric protein as for

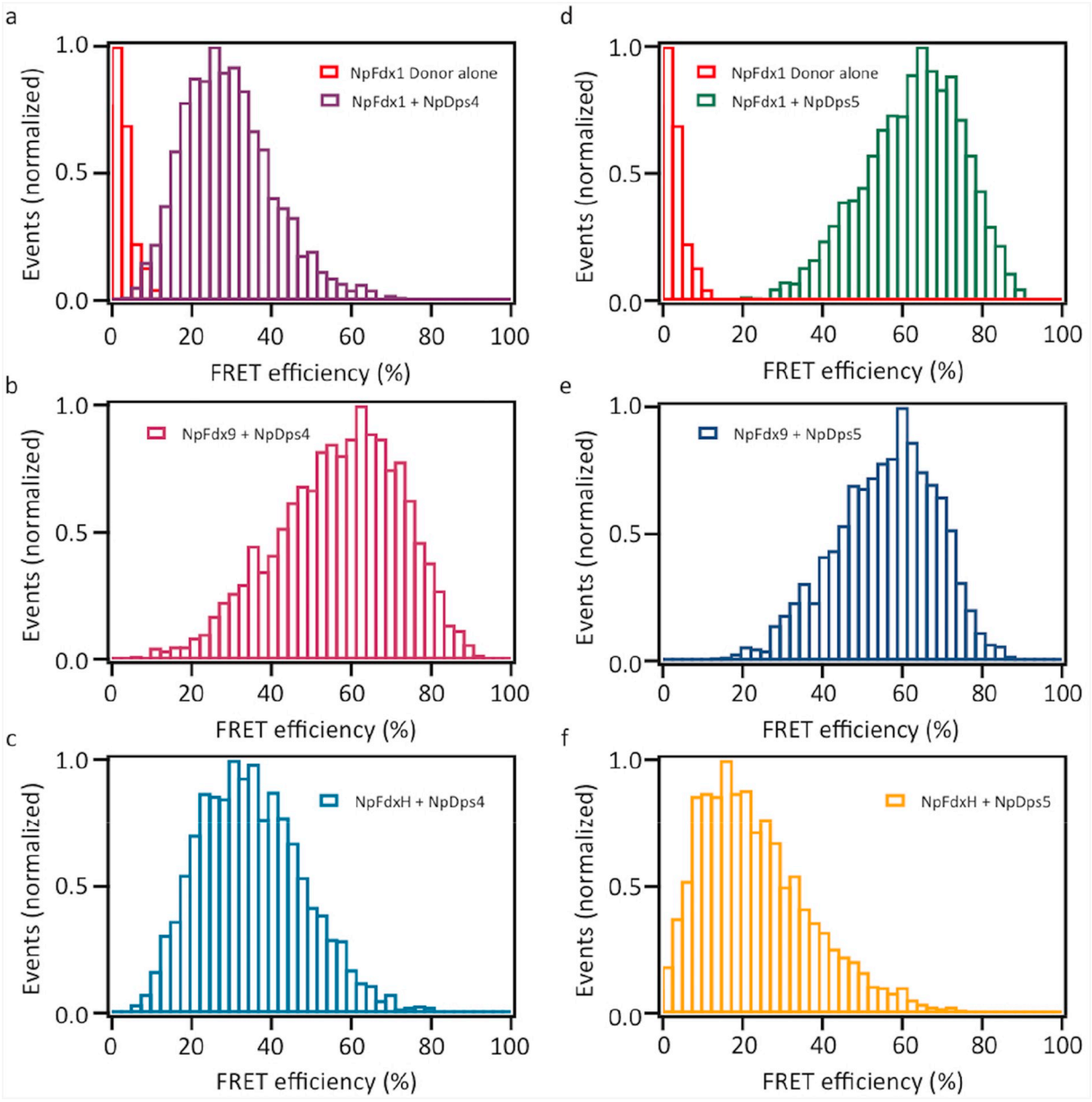

Fig. 5. Inter-FRET efficiency histograms of NpFdx variants and NpDps variants. The higher value in FRET histogram indicates the higher degree of compactness between proteins. Intermolecular FRET of NpFdx1-NpDps4 complex (a), NpFdx9-NpDps4 complex (b), NpFdxH-NpDps4 complex (c), NpFdx1-NpDps5 complex (d), NpFdx9-NpDps5 complex (e), and NpFdxH-NpDps4 complex (f) in comparison with NpFdx1 donor alone. In FRET histograms corresponding NpFdx proteins labeled with only donor fluorophore was used as a reference. Gaussian distributions were used to fit the data (data not shown). All experiments were carried out at 21 °C, at pH 6.0.

typical Dps, and not a 24-meric protein complex as for typical Bfr. Dodecameric structures as those expected for Dps proteins have been found among proteins with Bfr specific features, for example in the bacterium *Bacteroides fragilis* [55]. These proteins are categorized as Dps-like proteins, and NpDps5 relates structurally to those. It has been suggested that the Dps-like protein is an evolutionary link within the ferritin superfamily that connects dodecameric Dps to the Bfr 24-mer [55].

DLS results showed that NpDps4 and NpDps5 have individual optimal pH ranges for stability and multimerization in solution. Both NpDps form high molecular complexes between pH 5.0 to 8.0, whereas at pH 3.0 and pH 9.0 they are likely completely denatured (Fig. 2b). Size exclusion chromatography (Fig. S3) as well as FCS results supported these observations and confirmed that NpDps4 and EcDps were stable in their multimeric states at pH 6.0 and at pH 8.0, while NpDps5 appeared in higher and lower multimeric states at pH 6.0 and at pH 8.0 respectively. The dissociation at alkaline conditions does not seem to be due to total degradation, since predominant multimeric states were identified for both NpDps with all these complementary methods for determination of size. Therefore, we suggest that the dissociation of the multimeric form is pH-dependent. In general, the dodecameric shape of Dps proteins has been shown to be important for DNA binding, iron incorporation, and circumventing the Fenton reaction [15]. The realization of the individual pH dependences of the dodecameric structures was used to design the interactions studies and to interpret the results of these studies.

4.2. NpDps4 and NpDps5 show interaction with DNA

We found that both NpDps4 and NpDps5 interact with DNA in a pH

dependent fashion. Actually, this was a surprising result since NpDps5 is structurally similar to Bfr [20] which is a heme containing proteins not known to bind DNA. DpsA from *Synechococcus* sp. strain PCC 7942, another Dps protein with Bfr like features, has also been shown to interact with DNA [56]. The DNA binding features of DpsA as well as of NpDps5 could be explained as an evolutionary link between Bfr and Dps protein family.

Both NpDps4 and NpDps5 interacted with DNA at pH 6.0 in the gel-based EMSA experiments, but did not show binding at pH 7.0. In contrast the FCS data show NpDps specific pH dependent DNA binding. NpDps4 interacts with DNA at both pH 6.0 and at pH 8.0 while NpDps5 only show complex formation at pH 6.0. It may be that the electrostatic interaction, which is the common basis for DNA and Dps interaction [57], is impeded by the external electrical field that is applied during EMSA, a method that has to be regarded as more invasive as compared to FCS. The pattern for NpDps5-DNA interaction seen in the FCS experiments correlates with the loss of dodecameric structure of NpDps5 at pH 8.0 indicating the importance of the dodecamer structure for DNA-binding, at least *in vitro*.

The general mechanism of DNA binding by Dps proteins was provided for *E. coli* Dps, which carries three lysine residues at its N-terminus, that can be positively charged under physiological pH, and there upon forms large Dps-DNA complexes *in vitro* [57]. NpDps4 and NpDps5 exhibit a weaker DNA binding affinity as compared to the control EcDps (Fig. 3a, b). The poor NpDps4-DNA interaction is not easily explained by electrostatic properties, but the low number of positively charged amino acids in its terminal tail may be of significance (one arginine in the N-, one lysine at the C-terminus). Since both N- and C-termini are naturally short in NpDps5, the protein surface charges might be more relevant for NpDps5-DNA complex formation, as proposed for the Dps from *Helicobacter pylori* [58]. This biochemical property is dependent on pH that will modulate the overall protonation of the protein, which could lead to gain or loss of interaction [15]. While our study does not focus on this hypothesis, it is nevertheless an interesting avenue to pursue in a future study.

The long-standing hypothesis that DNA-binding would physically protect DNA from hydroxyl radicals (OH·), a ROS that is produced by the Fenton reaction, appears to be rather indefensible since many Dps proteins have been identified to protect DNA from this reaction without the capability to interact with DNA [59]. Therefore, it is likely that DNA binding fulfils other physiological roles such as DNA compaction [6] or physical protection from higher temperatures [60]. Dynamic state of DNA topology is essential for genome condensation in bacteria and has been studied *in vitro* for the gram-negative prokaryote *E. coli* [57] and the gram-positive *Staphylococcus aureus* [61]. As *N. punctiforme* in total contains five different Dps proteins, of which NpDps2, NpDps3 [43], NpDps4 and NpDps5 can form DNA-Dps complexes, it remains to be shown if any of these DNA-binding capabilities are of physiological relevance.

4.3. NpFdx proteins are possible electron donors for NpDps

NpFdx proteins interact with NpDps4 and NpDps5, indicating a potential role of these electron transfer proteins in redox activities of NpDps. Homologs of NpFdx1, NpFdx9 and NpFdxH act as electron donors in microalgae [29,30,62]. A homologue of NpFdx1 in *Chlamydomonas reinhardtii*, PetF acts as an electron carrier and plays a crucial role in the efficient electron transfer between Photosystem I (PSI) and the [FeFe] hydrogenase HydA1 [63,64]. FdxH is a heterocyst localized protein and has been shown to function as an electron donor to nitrogenase [65]. FdxH takes electrons from PSI in the light but can also be reduced by ferredoxin:NADPH oxidoreductase in darkness with the NADPH produced in oxidative pentose phosphate pathway [66]. These electron transfer reactions are based on the interaction of [Fe-S] centers from the donor (ferredoxin) to the acceptor protein (nitrogenase, PS I, hydrogenase). The [Fe−S] centers of the NpFdx1, NpFdx9 and NpFdxH from *N. punctiforme* were experimentally characterized and found to be consistent with those predicted from their primary protein structures, namely, NpFdx1 and NpFdxH containing [2Fe−2S] and NpFdx9 [4Fe−4S] centers. Previous studies on Fdx-based reduction of the stored iron in Bfr have shown that PaBfd interacts with, and reduce the iron core of PaBfr both *in vitro* and *in vivo* [10,34,35] and thus release iron. In this study we have shown that indeed NpFdx1, NpFdx9 and NpFdxH do interact with NpDps4 and NpDps5 under some of the tested conditions. The characteristics of the protein interactions are dependent on the Fdx-Dps couple. Based on the present FRET efficiencies the distance between the interacting fluorophores of NpFdx and NpDps can be calculated. NpFdx1 and NpFdxH are > 70 Å from NpDps4 (Fig. 5), while a distance of ~ 61 Å was found between NpFdx9 and NpDps4 (Fig. 5). The NpFdx proteins show different distances ranging from ~ 61 Å to 85 Å to NpDps5. As these values represent the distances between the FRET pair fluorophores coupled to the respective Dps and Fdx, only little can be inferred about the possibilities of electron transfer events, which occur at much smaller distances [67]. The exact location of the fluorophores, and the interaction surface between the protein partners is unknown, but displays crucial structural information to specifically determine the potential pathway of electron transfer.

However the NpFdx and NpDps interactions show unique binding induced modulation and does support complex formation. Further investigations are needed to conclude about their significance for reduction of stored iron that could be released to re-enter the metabolism. It should be noted that there are major dissimilarities between the investigated PaBfd:PaBfr and the NpFdx:NpDps complex. Bfrs contain heme groups on the 2-fold symmetry axis between two subunits, thus electronically connecting the protein exterior with the inner oxidized iron core. On the contrary the Dps proteins don't contain heme and the routes of electron transfer remain unknown. Additionally, the Bfd in complex with Bfr exhibit a distinct protein fold, which is different from the fold of other 2Fe−2S proteins and is dependent of a number of conserved amino acids for its stability [34]. In the studied cyanobacterial ferredoxins, these residues are not conserved and the structure of the NpFdx has yet to be determined. Establishing the electron transfer routes of iron storage and release in Dps is a major challenge that will have a huge impact on our understanding of iron homeostasis in cyanobacteria.

Transparency document

The Transparency document associated with this article can be found, in online version.

Acknowledgements

This work was supported by NordForsk NCoE program “NordAqua” (project # 82845), and the Swedish Energy Agency (project # 11674-5) (KS). Funding from Carl Tryggers Foundation (KS) and Sven and Lilly Lawski foundation (VKM) are also acknowledged. The research leading to these results has also received funding from the European Research Council (ERC) under the European Union's Seventh Framework Programme (FP7/2007-2013)/ERC Grant agreement 278242 (ExtendFRET) and the European Union's Horizon 2020 research and innovation programme (grant agreement No 723241 TryptoBoost).

Appendix A. Supplementary data

Supplementary data to this article can be found online at https://doi.org/10.1016/j.bbabio.2019.148063.

References

[1] P. Aisen, C. Enns, M. Wessling-Resnick, Chemistry and biology of eukaryotic iron metabolism, Int. J. Biochem. Cell Biol. 33 (2001) 940–959, https://doi.org/10.

1016/S1357-2725(01)00063-2.
[2] S.C. Andrews, A.K. Robinson, F. Rodriguez-Quinones, Bacterial iron homeostasis, FEMS Microbiol. Rev. 27 (2003) 215–237, https://doi.org/10.1016/S0168-6445(03)00055-X.
[3] S.J. Lippard, J.M. Berg, Principles of Bioinorganic Chemistry, University Science Books, Mill Valley, California, 1994, pp. 411–412.
[4] S. Shcolnick, N. Keren, Metal homeostasis in cyanobcateria and chloroplasts, balancing benefits and risks to the photosynthetic apparatus, Plant Physiol. 141 (2006) 805–810, https://doi.org/10.1104/pp.106.079251.
[5] N.E. Le Brun, A. Lewin, G.R. Moore, Formation of protein-coated iron minerals, Dalton Trans. 22 (2005) 3597–3610, https://doi.org/10.1039/b506071k.
[6] E. Chiancone, P. Ceci, The multifaceted capacity of Dps proteins to combat bacterial stress conditions: detoxification of iron and hydrogen peroxide and DNA binding, Biochim. Biophys. Acta 1800 (2010) 798–805, https://doi.org/10.1016/j.bbagen.2010.01.013.
[7] A. Ilari, S. Stefanini, E. Chiancone, D. Tsernoglou, The dodecameric ferritin from *Listeria innocua* contains a novel inter subunit iron-binding site, Nat. Struct. Biol. 7 (2000) 38–43, https://doi.org/10.1038/71236.
[8] E. Papinutto, W.G. Dundon, N. Pitulis, R. Battistutta, C. Montecucco, G. Zanotti, Structure of two iron-binding proteins from *Bacillus anthracis*, J. Biol. Chem. 277 (2002) 15093–15098, https://doi.org/10.1074/jbc.M112378200.
[9] B. Ren, G. Tibbelin, T. Kajino, O. Asami, R. Ladenstein, The multi-layered structure of Dps with a novel di-nuclear ferroxidase center, J. Mol. Biol. 329 (2003) 467–477, https://doi.org/10.1016/s0022-2836(03)00466-2.
[10] S.K. Weeratunga, C.E. Gee, S. Lovell, Y. Zeng, C.L. Woodin, M. Rivera, Binding of *Pseudomonas aeruginosa* apobacterioferritin-associated ferredoxin to bacterioferritin B promotes heme mediation of electron delivery and mobilization of core mineral iron, Biochemistry 48 (2009) 7420–7431, https://doi.org/10.1021/bi900561a.
[11] S. Yasmin, S.C. Andrews, G.R. Moore, N.E. Le Brun, A new role for heme, facilitating release of iron from the bacterioferritin iron biomineral, J. Biol. Chem. 286 (2011) 3473–3483, https://doi.org/10.1074/jbc.M110.175034.
[12] A. Martinez, R. Kolter, Protection of DNA during oxidative stress by the nonspecific DNA-binding protein Dps, J. Bacteriol. 179 (1997) 5188–5194, https://doi.org/10.1128/jb.179.16.5188-5194.1997.
[13] G. Zhao, P. Ceci, A. Ilari, L. Giangiacomo, T.M. Laue, E. Chiancone, N.D. Chasteen, Iron and hydrogen peroxide detoxification properties of DNA-binding protein of *Escherichia coli*, J. Biol. Chem. 277 (2002) 27689–27696, https://doi.org/10.1074/jbc.M202094200.
[14] S. Nair, S.E. Finkel, Dps protects cells against multiple stresses during stationary phase, J. Bacteriol. 186 (2004) 4192–4198, https://doi.org/10.1128/JB.186.13.4192-4198.2004.
[15] P. Ceci, A. Ilari, E. Falvo, L. Giangiacomo, E. Chiancone, Reassessment of protein stability, DNA binding, and protection of *Mycobacterium smegmatis* Dps, J. Biol. Chem. 280 (2005) 34776–34785, https://doi.org/10.1074/jbc.M502343200.
[16] A. Grove, S.P. Wilkinson, Differential DNA binding and protection by dimeric and dodecameric forms of the ferritin homolog Dps from *Deinococcus radiodurans*, J. Mol. Biol. 347 (2005) 495–508, https://doi.org/10.1016/j.jmb.2005.01.055.
[17] M. Su, S. Cavallo, S. Stefanini, E. Chiancone, N.D. Chasteen, The so-called *Listeria innocua* ferritin is a Dps protein, iron incorporation, detoxification, and DNA protection properties, Biochemistry. 44 (2005) 5572–5578, https://doi.org/10.1021/bi0472705.
[18] M. Castruita, M. Saito, P.C. Schottel, L.A. Elmegreen, S. Myneni, E.I. Stiefel, F.M.M. Morel, Overexpression and characterization of an iron storage and DNA-binding Dps protein from *Trichodesmium erythraeum*, Appl. Environ. Microbiol. 72 (2006) 2918–2924, https://doi.org/10.1128/AEM.72.4.
[19] A. Latifi, M. Ruiz, C.C. Zhang, Oxidative stress in cyanobacteria, FEMS Microbiol. Rev. 33 (2009) 258–278, https://doi.org/10.1111/j.1574-6976.2008.00134.x.
[20] M. Ekman, G. Sandh, A. Nenninger, P. Oliveira, K. Stensjö, Cellular and functional specificity among ferritin-like proteins in the multicellular cyanobacterium *Nostoc punctiforme*, Environ. Microbiol. 16 (2014) 829–844, https://doi.org/10.1111/1462-2920.
[21] V.K. Moparthi, X. Li, K. Vavitsas, I. Dzhygyr, G. Sandh, K. Stensjö, The two Dps proteins, Npun_F3730 and Npun_F6212, are involved in light-induced oxidative stress tolerance in the N_2 fixing cyanobacterium, *Nostoc punctiforme*. Biochim. Biophys. Acta. Bioenergetics 1857 (2016) 1766–1776, https://doi.org/10.1016/j.bbabio.2016.08.003.
[22] X. Li, H. Mustila, A. Magnuson, K. Stensjö, Homologous overexpression of NpDps2 and NpDps5 increases the tolerance of oxidative stress in the multicellular cyanobacterium *Nostoc punctiforme*, FEMS Microbiol. Lett. 365 (2018) 1–8, https://doi.org/10.1093/femsle/fny198.
[23] J.C. Meeks, J. Elhai, T. Thiel, M. Potts, F. Larimer, J. Lamerdin, P. Predki, R. Atlas, An overview of the genome of *Nostoc punctiforme*, a multicellular, symbiotic cyanobacterium, Photosynth. Res. 70 (2001) 85–106, https://doi.org/10.1023/A:1013840025518.
[24] F. Alaleona, S. Franceschini, P. Ceci, A. Ilari, E. Chiancone, *Thermosynechococcus elongatus* DpsA binds Zn(II) at a unique three histidine-containing ferroxidase center and utilizes O2 as iron oxidant with very high efficiency, unlike the typical Dps proteins, FEBS J. 277 (2010) 903–917, https://doi.org/10.1111/j.1742-4658.2009.07532.x.
[25] C. Howe, V.K. Moparthi, F.M. Ho, K. Persson, K. Stensjö, The Dps4 from *Nostoc punctiforme* ATCC 29133 is a member of His-type FOC containing Dps protein class that can be broadly found among cyanobacteria, PLoS One 14 (2019) e0218300, , https://doi.org/10.1371/journal.pone.0218300.
[26] S.Y. Ow, J. Noirel, T. Cardona, A. Taton, P. Lindblad, K. Stensjö, P.C. Wright, Quantitative overview of N_2 fixation in *Nostoc puntiforme* ATCC 29133 through cellular enrichments and iTRAQ shotgun proteomics, J. Proteome Res. 8 (2009) 187–198, https://doi.org/10.1021/pr700604v.
[27] A.M. Muro-Pastor, W.R. Hess, Heterocyst differentiation: from single mutants to global approaches, Trends Microbiol. 20 (2012) 548–557, https://doi.org/10.1016/j.tim.2012.07.005.
[28] H. Sticht, P. Rosch, The structure of iron-sulfur proteins, Prog. Biophys. Mol. Biol. 70 (1998) 95–136, https://doi.org/10.1016/S0079-6107(98)00027-3.
[29] G. Hanke, P. Mulo, Plant type ferredoxins and ferredoxin-dependent metabolism, Plant Cell Environ. 36 (2013) 1071–1084, https://doi.org/10.1111/pce.12046.
[30] C.C. Chauvat, F. Chauvat, Function and regulation of ferredoxins in the cyanobacterium *Synechocystis* PCC6803: recent advances, Life. 4 (2014) 666–680, https://doi.org/10.3390/life4040666.
[31] H. Böhme, B. Schrautemeier, Comparative characterization of ferredoxins from heterocysts and vegetative cells of *Anabaena variabilis*, Biochim. Biophys. Acta 891 (1987) 1–7, https://doi.org/10.1016/0005-2728(87)90076-4.
[32] B. Schrautemeier, H. Bohme, A distinct ferredoxin for nitrogen fixation isolated from heterocysts of the cyanobacterium *Anabaena variabilis*, FEBS Lett. 184 (1985) 304–308, https://doi.org/10.1016/0014-5793(85)80627-X.
[33] M.A. Quail, P. Jordan, J.M. Grogan, J.N. Butt, M. Lutz, A.J. Thomson, S.C. Andrews, J.R. Guest, Spectroscopic and voltammetric characterization of the bacterioferritin-associated ferredoxin of *Escherichia coli*, Biochem. Biophys. Res. Commun. 229 (1996) 635–642, https://doi.org/10.1006/bbrc.1996.1856.
[34] H. Yao, Y. Wang, S. Lovell, R. Kumar, A.M. Ruvinsky, K.P. Battaile, I.A. Vakser, M. Rivera, The structure of the BfrB-Bfd complex reveals protein-protein interactions enabling iron release from bacterioferritin, J. Am. Chem. Soc. 15 (134) (2012) 13470–13481, https://doi.org/10.1021/ja305180n.
[35] K. Eshelman, H. Yao, A.N.D. Punchi Hewage, J.J. Deay, J.R. Chandler, M. Rivera, Inhibiting the BfrB:Bfd interaction in *Pseudomonas aeruginosa* causes irreversible iron accumulation in bacterioferritin and iron deficiency in the bacterial cytosol, Metallomics 9 (2017) 646–659, https://doi.org/10.1039/c7mt00042a.
[36] T. Haikarainen, A.C. Papageorgiou, Dps-like proteins: structural and functional insights into a versatile protein family, Cell. Mol. Life Sci. 67 (2010) 341–351, https://doi.org/10.1007/s00018-009-0168-2.
[37] E.L. Campbell, H. Christman, J.C. Meeks, DNA microarray comparisons of plant factor- and nitrogen deprivation-induced hormogonia reveal decision-making transcriptional regulation patterns in *Nostoc punctiforme*, J. Bacteriol. 190 (2008) 7382–7391, https://doi.org/10.1128/JB.00990-08.
[38] R.G. Taylor, D.C. Walker, R.R. Mclnnes, *E. coli* host strains significantly affect the quality of small scale plasmid DNA preparations used for sequencing. Nucleic. Acids. Res. 21 (1993) 1677–1678. doi:https://doi.org/10.1093/nar/21.7.1677.
[39] B. Miroux, J.E. Walker, Over-production of proteins in *Escherichia coli*: mutant hosts that allow synthesis of some membrane proteins and globular proteins at high levels, J. Mol. Biol. 260 (1996) 289–298, https://doi.org/10.1006/jmbi.1996.0399.
[40] R. Rippka, Isolation and purification of cyanobacteria, Methods Enzymol. 167 (1988) 3–27, https://doi.org/10.1016/0076-6879(88)67004-2.
[41] A.V. Bryksin, I. Matsumura, Overlap extension PCR cloning: a simple and reliable way to create recombinant plasmids, BioTechniques. 48 (2010) 463–465, https://doi.org/10.2144/000113418.
[42] S.W. Edward, Chemical transformation of *E. coli*, in: N. Casali, A. Preston (Eds.), *E. coli* Plasmid Vectors, Humana press, Methods. Mol. Biol. Springer, 2003, pp. 49–53.
[43] C. Howe, F.M. Ho, A. Nenninger, P. Raleiras, K. Stensjö, Differential biochemical properties of three canonical Dps proteins from the cyanobacterium *Nostoc punctiforme* suggest distinct cellular functions, J. Biol. Chem. 293 (2018) 16635–16646, https://doi.org/10.1074/jbc.RA118.002425.
[44] U.K. Laemmli, Cleavage of structural proteins during the assembly of the head of bacteriophage T4, Nature. 227 (1970) 680–685, https://doi.org/10.1038/227680a0.
[45] T. Fujisawa, R. Narikawa, S. Maeda, S. Watanabe, Y. Kanesaki, K. Kobayashi, J. Nomata, M. Hanaoka, M. Watanabe, S. Ehira, CyanoBase: a large-scale update on its 20th anniversary, Nucleic Acids Res. 45 (2016) 551–554, https://doi.org/10.1093/nar/gkw1131.
[46] F. Sievers, A. Wilm, D. Dineen, T.J. Gibson, K. Karplus, W. Li, R. Lopez, H. McWilliam, M. Remmert, J. Söding, Fast, scalable generation of high-quality protein multiple sequence alignments using Clustal Omega, Mol. Syst. Biol. 7 (2011) 539–544, https://doi.org/10.1038/msb.2011.75.
[47] S.B. Moparthi, G. Thieulin-Pardo, P. Mansuelle, H. Rigneault, B. Gontero, J. Wenger, Conformational modulation and hydrodynamic radii of CP12 protein and its complexes probed by fluorescence correlation spectroscopy, FEBS J. 281 (2014) 3206–3217, https://doi.org/10.1111/febs.12854.
[48] K. Brzoska, S. Meczynska, M. Kruszewski, Iron-sulfur cluster proteins:electron transfer and beyond, Acta Biochim. Pol. 53 (2006) 685–691.
[49] R. Schmidt, R. Zahn, B. Bukau, A. Mogk, ClpS is the recognition component for *Escherichia coli* substrates of the N-end rule degradation pathway, Mol. Microbiol. 72 (2009) 506–517, https://doi.org/10.1111/j.1365-2958.2009.06666.x.
[50] A. Shevchenko, M. Wilm, O. Vorm, M. Mann, Mass spectrometric sequencing of proteins from silver-stained polyacrylamide gels, Anal. Chem. 68 (1996) 850–858, https://doi.org/10.1021/ac950914h.
[51] Stout CD (2001) Ferredoxins containing two different Fe/S centers of the forms [4Fe-4S] and [3Fe-4S]. Handbook of Metalloproteins (Messerschmidt AHR, Poulos T, Wieghardt K, ed.) John Wiley & Sons, Ltd, United Kingdom. 560-573.
[52] R.P. Chowdhury, M. Vijayabaskar, S. Vishveshwara, D. Chatterji, Molecular mechanism of in vitro oligomerization of Dps from *Mycobacterium smegmatis*: mutations of the residues identified by “Interface Cluster” analysis, Biochemistry 47 (2008) 11110–11117, https://doi.org/10.1021/bi801158e.
[53] R. Fan, A.L. Boyle, V.V. Cheong, S.L. Ng, B.P. Orner, A helix swapping study of two protein cages, Biochemistry 48 (2009) 5623–5630, https://doi.org/10.1021/bi900387t.

[54] M. Almiron, A.J. Link, D. Furlong, R. Kolter, A novel DNA-binding protein with regulatory and protective roles in starved *Escherichia coli*, Genes Dev. 6 (1992) 2646–2654, https://doi.org/10.1101/gad.6.12b.2646.
[55] G.H. Gauss, M.A. Reott, E.R. Rocha, M.J. Young, T. Douglas, C.J. Smith, C.M. Lawrence, Characterization of the *Bacteroides fragilis* bfr gene product identifies a bacterial DPS-like protein and suggests evolutionary links in the ferritin superfamily, J. Bacteriol. 194 (2012) 15–27, https://doi.org/10.1128/JB.05260-11.
[56] M.M.O. Pena, GS. Bullerjahn, The DpsA protein of *Synechococcus* sp. Strain PCC7942 is a DNA-binding hemoprotein, linkage of the Dps and bacterioferritin protein families, J. Biol. Chem, 270, 38 (1995) 22478–22482. doi:https://doi.org/10.1074/jbc.270.38.22478.
[57] P. Ceci, S. Cellai, E. Falvo, C. Rivetti, G. Rossi, E. Chiancone, DNA condensation and self-aggregation of *Escherichia coli* Dps are coupled phenomena related to the properties of the N-terminus, Nucleic Acids Res. 32 (2004) 5935–5944, https://doi.org/10.1093/nar/gkh915.
[58] P. Ceci, L. Mangiarotti, C. Rivetti, E. Chiancone, The neutrophil-activating Dps protein of *Helicobacter pylori*, HP-NAP, adopts a mechanism different from *Escherichia coli* Dps to bind and condense DNA, Nucleic. Acids. Res. 35 (2007) 2247–2256. doi:https://doi.org/10.1093/nar/gkm077.
[59] G. Bellapadrona, M. Ardini, P. Ceci, S. Stefanini, E. Chiancone, Dps proteins prevent Fenton-mediated oxidative damage by trapping hydroxyl radicals within the protein shell, Free Radic. Biol. Med. 48 (2010) 292–297, https://doi.org/10.1016/j.freeradbiomed.2009.10.053.
[60] E. Chiancone, Dps Proteins, an Efficient Detoxification and DNA Protection Machinery in the Bacterial Response to Oxidative Stress, in: Rendiconti Lincei, Scienze Fisiche e Naturali, Springer-Verlag Italia, 2008, pp. 261–270.
[61] K. Morikawa, R.L. Ohniwa, J. Kim, A. Maruyama, T. Ohta, K. Takeyasu, Bacterial nucleoid dynamics: oxidative stress response in *Staphylococcus aureus*, Genes Cells 11 (2006) 409–423, https://doi.org/10.1111/j.1365-2443.2006.00949.x.
[62] Y. Allahverdiyeva, M. Ermakova, M. Eisenhut, P. Zhang, P. Richaud, M. Hagemann, L. Cournac, E.M Aro, Interplay between flavodiiron proteins and photorespiration in *Synechocystis* sp. PCC 6803, J. Biol. Chem. 286 (2011) 24007–24014. doi:https://doi.org/10.1074/jbc.M111.223289.
[63] M. Winkler, S. Kuhlgert, M. Hippler, T. Happe, Characterization of the key step for light-driven hydrogen evolution in green algae, J. Biol. Chem. 284 (2009) 36620–36627, https://doi.org/10.1074/jbc.M109.053496.
[64] M. Winkler, A. Hemschemeier, J. Jacobs, S. Stripp, T. Happe, Multiple ferredoxin isoforms in *Chlamydomonas reinhardtii*- their role under stress conditions and biotechnological implications, Eur. J. Cell Biol. 89 (2010) 998–1004, https://doi.org/10.1016/j.ejcb.2010.06.018.
[65] H. Böhme, R. Haselkorn, Molecular cloning and nucleotide sequence analysis of the gene coding for heterocyst ferredoxin from the cyanobacterium *Anabaena* sp. strain PCC 7120, Mol. Gen. Genet. 214 (1988) 278–285, https://doi.org/10.1007/BF00337722.
[66] H. Bothe, O.M. Schmitz, M.G. Yates, E. William, 2010, nitrogen fixation and hydrogen metabolism in cyanobacteria, Micro. Mol. Biol. Rev. 74 (2010) 529–551, https://doi.org/10.1128/MMBR.00033-10.
[67] C.C. Page, C.C. Moser, P.L. Dutton, Mechanism for electron transfer within and between proteins, Curr. Opin. Chem. Biol. 7 (2003) 551–556, https://doi.org/10.1016/j.cbpa.2003.08.005.